Powder Technology 434 (2024) 119353

Contents lists available at ScienceDirect

Powder Technology

journal homepage: www.journals.elsevier.com/powder-technology

Rate dependence in adhesive particle–particle contacts affect ceramic suspension bulk flow behavior

Zohreh Farmani, Joshua A. Dijksman *

Physical Chemistry and Soft Matter, Wageningen University & Research, Stippeneng 4, Wageningen, 6708 WE, The Netherlands
Van der Waals-Zeeman Institute, Institute of Physics, University of Amsterdam, Science Park 904, Amsterdam, 1098 XH, The Netherlands

HIGHLIGHTS

- Molecular to macro-scale adhesive behavior of the ceramic microparticles is studied.
- Colloid probe atomic force microscopy (CP-AFM) reveals two time scales in adhesion.
- Rheology measurements suggest that adhesion affects flow behavior.
- Changing pH affects adhesive properties of ceramic particles.

GRAPHICAL ABSTRACT

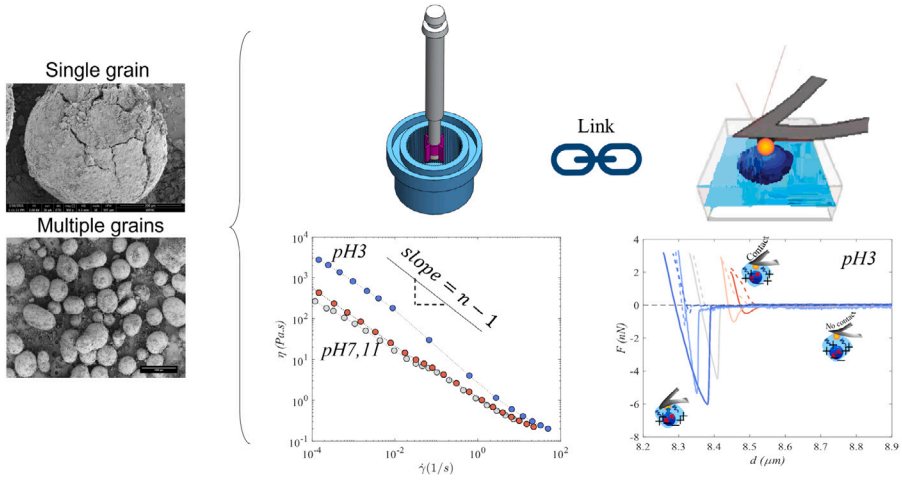

ARTICLE INFO

Keywords:
Adhesive properties
Colloidal probe atomic force microscopy
CP-AFM
Ceramic suspension

ABSTRACT

Particle–fluid mixtures are known for displaying a wide variety of interesting flow mechanisms, such as thickening and thinning under shear. It is now becoming increasingly evident that even molecular scale effects are relevant for this macroscopic flow behavior of suspensions. Here we show that even 50 μm ceramic beads in a non-density matched solvent are affected by the pH of the solvent. We trace the origin of the pH dependence to the contact mechanics using colloidal probe atomic force microscopy (CP-AFM). The gel-like structure of the pH 3 samples suggests that adhesion effects play a major role, but which adhesion timescale competes with shear rate to affect the rheology is not obvious. We test here two time scales in the contact mechanics: total contact time t_c and contact retraction speed v_r. We observe that contact time is the most important variable to correlate with rheology. The ceramic particle suspension so serves as a model system to help understand which adhesive mechanism affects flow behavior in the suspension.

* Corresponding author at: Van der Waals-Zeeman Institute, Institute of Physics, University of Amsterdam, Science Park 904, Amsterdam, 1098 XH, The Netherlands.
E-mail address: j.a.dijksman@uva.nl (J.A. Dijksman).

https://doi.org/10.1016/j.powtec.2023.119353
Received 16 March 2023; Received in revised form 25 November 2023; Accepted 31 December 2023
Available online 3 January 2024

1. Introduction

Particle–fluid mixtures are of great importance in many areas of industrial processing, e.g. in the food industry, oil recovery, and the ceramics industry [1]. Particle suspensions are a class of complex fluids that exhibit a wide range of flow behavior depending on the applied shear rate and particle concentration. Experimental studies have demonstrated the unique behavior of fluid suspensions including shear-thinning, shear-thickening, and yield stresses [2–4]. Shear thinning is the non-Newtonian behavior of fluids whose viscosity decreases under shear rate, attributed to interactions between particles and between particles and fluid, and to changes in microstructure under shear [5,6]. The origin of shear thinning suspensions could be the restructuring of particles under shear, frictional and adhesive interactions between particles. Gadala-Maria and Acrivos have already studied the mechanisms of particle structuring that induce the shear thinning response [7]. The important role of interparticle interactions in determining shear thinning behavior is also addressed in many studies that have appeared since then. For example, Chatte et al. showed that the frictional contacts between particles are the primary mechanism responsible for the shear thinning behavior of the suspension [2]. Vázquez-Quesada et al. studied causes of shear-thinning in non-colloidal suspensions at a 40% volume fraction. Using silicone oil and glycerine/water mixtures with particles, they found that hidden high shear rates between particles contribute to shear-thinning in non-Newtonian matrices. The glycerine/water system implies a separate mechanism involving variable interparticle friction. This observation confirms their previous findings [3]. Another study that discussed the shear-thinning in non-Brownian suspension by particle frictions is Lobry et al. [6]. Simulations, incorporating a load-dependent friction coefficient, align well with viscosity measurements in silicon oil with polystyrene particles. The proposed model suggests that as shear stress increases, friction decreases, leading to viscosity reduction. Additionally, the model provides a means to calculate microscopic friction coefficients from rheometric measurements. Tanner et al. have also examined the role of friction in non-colloidal suspensions using a model [8]. They presented a model for non-colloidal suspensions, dividing viscosity into frictionless and frictional components. It demonstrates how friction feedback increases viscosity, applies to volume fractions up to 0.5, and proves useful for deducing friction coefficients from experimental data, for spheres in silicone oil. On the other hand, Amiri et al. changed the properties of the solvent in which the particles are suspended, and found that the adhesive contacts can dominate the rheology of the suspension [9], as demonstrated in biological fluids such as blood [10] as well as silica particle suspensions [11].

Dense suspensions usually age due to structural dynamics. Recent studies on aging in dense suspensions unveil two processes: structural dynamics-driven aging and contact-controlled aging, where stiffening solid–solid contacts impact shear modulus. This is significant when Coulombic interactions are screened out, challenging existing views on aging dynamics across various materials. Bonnaci et al. introduced contact-controlled aging, where solid–solid contacts progressively stiffen, affecting shear modulus aging in materials like silica and polymer latex suspensions [12]. This process becomes relevant with moderate ion concentrations. In another study, these authors investigated the yield stress aging in suspensions with irreversible interparticle contacts. Through optical tweezer tests, they identified a time-dependent rolling threshold that governs yield stress and aging kinetics, establishing a constitutive relation applicable to diverse colloidal systems [13]. In addition, several studies addressed the behavior of non-brownian dense suspensions under the oscillatory rheology. Martone et al. discovered that the apparent complex viscosity depends not only on the amplitude of applied strain but also on the angular frequency, challenging conventional expectations for such suspensions [14]. The study identifies two regimes based on the applied strain: one with frequency-dependent viscosity driven by shear-induced diffusion and another with rate-independent viscosity. This finding holds across concentrations, revealing concentration-independent physics underlying the rate dependence. Park et al. also studied the oscillatory rheology in suspensions. They found out that even at small strain amplitudes, the stress response deviates from linear behavior. Particularly, the stress component in phase with the strain experiences a significant decay. Additionally, the apparent complex viscosity demonstrates a nonmonotonic dependence on strain amplitude for volume fractions exceeding 0.2.

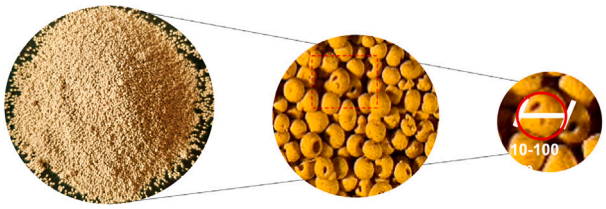

Fig. 1. The powder of interest. Several length scales are indicated. The ceramic microparticles are hollow spheres with size distribution between few μm to 600 μm.

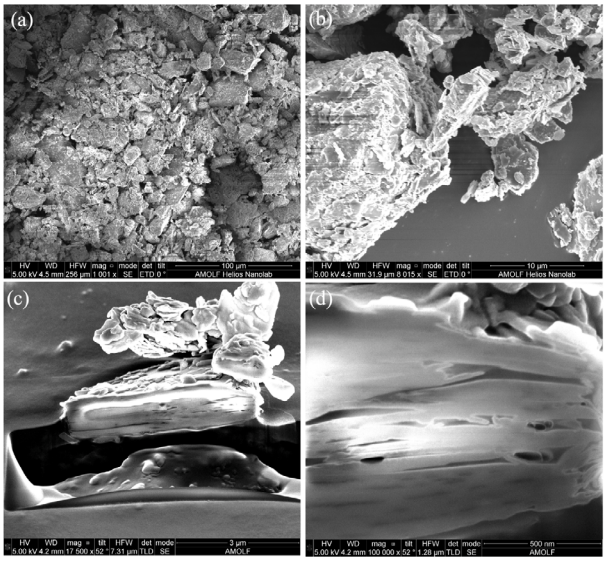

Fig. 2. Microscopy images of ceramic micro-particles with size of < 64 μm. (a) SEM image with 100 μm magnification showing irregular shaped powders, (b) zoom in to the image a with 10 μm magnification showing the surface structure of one tiny particle, (c) FIB-SEM image showing a cut through one single particle showing the internal structure of the particle, and (d) zoom in to the right side of image c showing the layered/porous structure of the particle with nm thickness.

Despite the enormous research efforts to decipher certain mechanisms that determine the flow behavior of particle suspensions [15–18], it is still unclear how exactly the morphology of the particle surface, the surface functional groups, as well as the physical properties of the suspending media influence the particle interactions and thus the rheology. To unravel the effects of the surface morphology of the particles and the physical properties of the suspending media, effects at the molecular level are relevant to the macroscopic flow behavior of suspensions. Atomic force microscopy is a useful technique to study such molecular scale effects [19] and hence link the microscopic to the macroscopic flow behavior. Surface characterization techniques have made a significant contribution to our understanding of the mechanics and rheology of suspensions. Indeed, the applicability and usefulness of atomic force microscopy as an essential surface characterization technique is evident in several areas [20,21]. In the last 20 years, numerous studies have been conducted on the use of various techniques including atomic force microscopy (AFM) [22], colloidal probe atomic

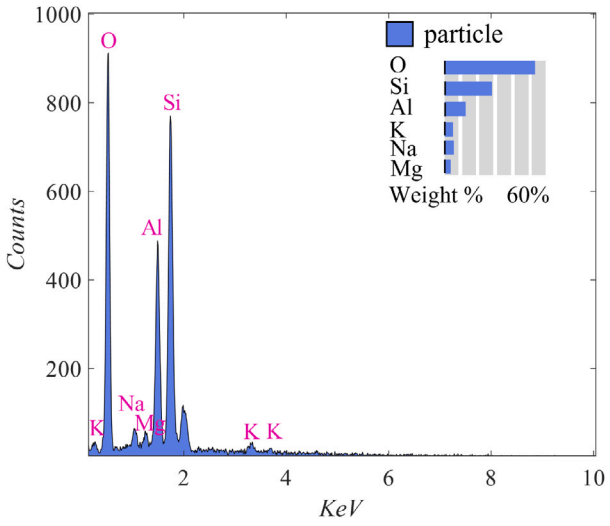

Fig. 3. EDX (elemental analysis) of the ceramic micro-particles.

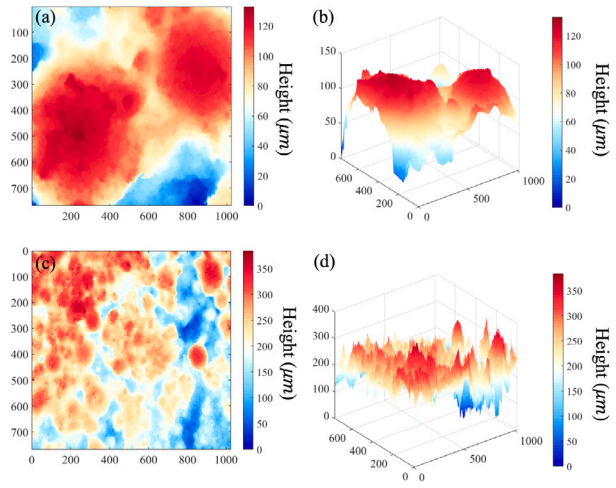

Fig. 4. Height maps showing the scale of surface roughness of ceramic microparticles at pH3, (a) 2d map with ×50 magnification, (b) surface profile with ×50 magnification, (c) 2d map with ×5 magnification, and (d) surface profile with ×5 magnification. The scale in the x-y plane is not calibrated; the numbers are in pixels.

force microscopy (CP-AFM) [23], local force spectroscopy (LFS) [24], chemical force microscopy (CFM) [25], etc.

We focus here on CP-AFM which is very popular for studying adhesion forces between two particles or a particle and a surface. In CP-AFM, a cantilever tip can be functionalized by glueing a μm-sized particle on top of it [26,27]. Functionalizing the cantilever is useful in the sense that one can use any desired material as a probe material; Using CP-AFM it is possible to determine the magnitudes and time-dependence of rupture forces, the estimation of the point of tip–sample contact, and the elastic modulus and plasticity of the material [28]. A huge amount of research related to CP-AFM has been conducted using well-defined surfaces, such as silica, mica, etc. For example, Bowen et al. [29], used CP-AFM to quantify the adhesion interaction between a silica sphere and a planar silica surface. The authors found that the experimentally measured adhesion forces depended on sample preparation and solution pH.

In addition to the works done on well-defined silica surfaces [29, 30], some studies have focused on investigating the adhesion force on natural mineral surfaces. In 2012, Filby et al. [31], studied the interaction of carboxylated latex colloids with several mineral surfaces (quartz, muscovite, biotite, K-feldspar, apatite and titanite) in aqueous sample solutions with pH ranging from 2 to 10 at constant ionic strength. The adsorption of charged colloids on natural mineral surfaces is still poorly understood. Therefore further studies are needed to reveal some phenomena that occur when a colloid interacts with a mineral surface. It is also important to understand and characterize the fundamental interactions between different tips and sample surfaces under different environmental conditions. For instance, the adhesion force is sensitive to the surface energies of the materials with which the tips are coated, e.g., the adhesion force between a gold-coated tip and a mica surface is much greater than that between a paraffin-coated tip and a mica surface [32].

Here we emphasize that the molecular scale effects in silica particles studied by CP-AFM is the key to understanding the fluid mechanics and rheology of suspensions of silica particles. The microscopic effects revealed by CP-AFM not only offer the possibility to explain the observations in the flow curves, but are also crucial for the understanding of pH-dependent adhesive contacts. We use colloidal probe atomic force microscopy CP-AFM to trace the origin of pH dependence to contact mechanics. We measure the pH-induced adhesion force by tuning the interparticle interactions in systems of ceramic microparticles and commercial silica particles. Our findings in contact mechanics and bulk rheology should provide a fundamental understanding of how ceramic particles with complex surface morphology and chemistry behave in slurries, which may provide new insights to the ceramic industry, for example.

2. Materials and methods

2.1. Particle suspensions

We used commercial silica particles and ceramic microparticles (Fig. 1) supplied by SACMI company based in Imola, Italy. The particle size distribution of the ceramic micro-particles is between few μm to 600 μm. We used the smallest fraction (<63 μm) in both rheology and AFM measurements. The surface and bulk morphology was evaluated through Scanning Electron Microscopy (SEM) (Fig. 2a,b) and Focused Ion Beam etching (FIB-SEM) (Fig. 2c,d), whereas the average elemental composition of the minerals was obtained from Energy Dispersive X-ray Analysis (EDX) (Fig. 3). Fig. 2 shows that the ceramic particles have a complex surface structure which might show plasticity and deformation when in contact. Fig. 2a,b are images from chromium-coated powders of size <63 μm. Fig. 2c,d is the same chromium-coated powder. However we did platinum deposition on a single spot and then focused an 30 kV and 93 pA ion beam to make a cut through the particle. It shows that the particle has a layered or porous structure with pores of nm in size. The ceramic particles consist of almost 70% SiO_2 and 30% Al_2O_3, estimated by the EDX measurements (Fig. 3). The error of the EDX measurements is estimated as 0.5–1.1%, depending on the sample matrix and acceleration voltage. We dispersed the required amount of particle mass to achieve a given volume fraction ($\phi = 0.4$) in milli-Q water with different pH=3,7,11. We thereafter mixed them using a high shear mixer. The pH is tuned using a pH-meter (Schott) before and after mixing. Further increase of the particle concentration in water led to inhomogeneities and the inability of evenly dispersing the solids into the solvent. We performed rheology measurements immediately after preparing the suspensions.

The presence of (sub) surface roughness on the ceramic particles can influence the interactions. Therefore, we have also performed surface profilometry to measure the scale of roughness on ceramic substrate. Fig. 4 shows the height map for one sample with pH=3. The surface roughness is approximately in the range of 120 μm.

2.2. Macro-scale measurements: rheology

For the macro-scale suspension rheology measurements, we used an Anton-Paar 301 rheometer with a vane-cup geometry (Fig. 5). We

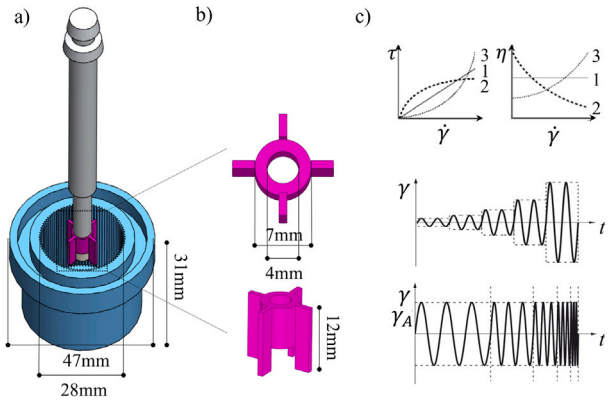

Fig. 5. Schematic of the geometry for rheological measurements, (a) cup-vane with inner diameter D_{ic} = 28 mm, outer diameter D_{oc} = 47 mm, and cup height of H_c = 31 mm, (b) zoom into the vane of D_{iv} = 4 mm, D_{ov} = 7 mm with 4 blades of height H_v = 12 mm, and (c) schematic of the performed rheological measurements: *rotational measurements* including steady shear which gives shear stress τ and viscosity η as a function of shear rate $\dot{\gamma}$, and *oscillation measurements* including amplitude sweep (constant frequency f, ramp in strain γ) and frequency sweep (constant γ (γ_A), ramp in f).

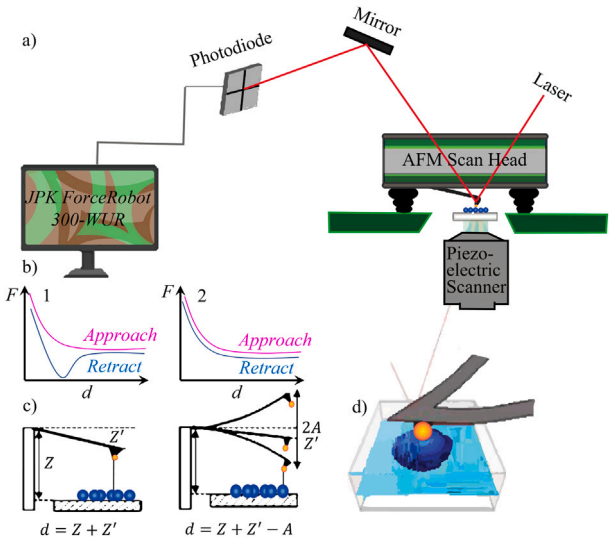

Fig. 6. The colloidal probe atomic force microscopy CP-AFM. (a) sketch of the CP-AFM designed for force spectroscopy, (b) typical force-distance F-d plots obtained from CP-AFM, 1-adhesive system, 2-non-adhesive system, (c) approach and retract of the functionalized cantilever with colloidal particle with respect to a substrate covered by ceramic microparticles. Here we can measure the distance d with respect to the substrate, and force F with deflection of the beam, and (d) functionalized cantilever and ceramic microparticle are submersed in water.

used a pH meter next to the rheometer to verify and tune the pH of the suspension. The procedure of the measurements is as follows: (1) interval 1: Pre-shear (shear rate ($\dot{\gamma}$)=10 1/s), wait for sedimentation (120 s, $\dot{\gamma}$=0), shear stress ramp (τ=0.01–10 Pa), (2) interval 2: Pre-shear ($\dot{\gamma}$=10 1/s), wait for sedimentation (120 s, $\dot{\gamma}$=0), amplitude sweep (γ=100-0.01%, frequency(f)=1 Hz), and (3) interval 3: Pre-shear ($\dot{\gamma}$=10 1/s), wait for sedimentation (120 s, $\dot{\gamma}$=0), frequency sweep (angular frequency (ω)=10-0.1rad/s, γ=0.01%).

We performed the rotational shear experiments to extract the viscosity η response of the suspension as we increase the shear rate $\dot{\gamma}$. From viscosity plot we can understand the resistance of the suspension to flow/deformation, which can then be correlated to the adhesive properties of the suspension; the more cohesive, the higher the viscosity. This resistance to flow can be due to the internal friction or cohesion. To study the visco-elastic behavior of the suspension, we performed oscillation tests. First we kept the frequency constant (f = 1 Hz) and swept the strain. The vane oscillates back and forth while recording the storage (G') and loss modulus (G'') [33]. Storage modulus G' (elastic portion) represents the stored deformation energy and loss modulus G'' (viscous portion) characterizes the deformation energy lost (dissipated) when flowing. Solid-like viscoelastic materials have a higher storage modulus than loss modulus $G' > G''$. Viscoelastic liquids then have a higher loss modulus than storage modulus $G'' > G'$ [34,35]. All measurements were done at room temperature (20 °C).

In amplitude sweep measurements, the length of the linear visco-elastic region (plateau at low strain γ) indicates the range in which the test can be performed without destroying the structure of the sample. The frequency sweep shows the time-dependent behavior of a sample in the non-destructive deformation range.

2.3. Micro-scale measurements: Colloidal probe atomic force microscopy, CP-AFM

We performed all microscopic measurements on a ForceRobot 300 (JPK), a type of atomic force microscope designed for force spectroscopy (Fig. 6) [36]. We used tipless cantilevers (MLCT-O10, Au reflective coating) with a nominal spring constant of k = 0.1 N m^{-1} and a nominal resonance frequency of 67 kHz. We functionalized the AFM cantilevers by gluing a spherical silica microparticle ($R \approx 4$ μm). Fig. 7 shows the procedure for functionalizing the cantilevers with a silica particle and the colloidal probe used in this work Fig. 7d. Cantilevers with excess glue were not used. Although the manufacturer describes spring constants for the cantilevers, the actual spring constant may deviate from this value by an order of magnitude. It is, therefore, necessary to determine the spring constant experimentally. Thus, we calibrated the spring constant (k = 0.1 N m^{-1}) of each cantilever with the thermal noise method using a correction factor of 0.251. We choosed cantilevers with low spring constant values to be sufficiently sensitive to forces in liquid. The maximum force applied by the cantilever reaches 30–35 nN. We also used < 63 μm ceramic microparticles on a glass substrate. We used a rubber ring to create a chamber between the probe holder and substrate to perform measurements in water. We first treated the AFM probes and substrates using a plasma cleaner to remove contaminants. We then rinsed the probe and substrate with water to deactivate their surfaces.

In a typical measurement, after setting up the probe, substrate and the rubber ring, we inject water with a certain pH to the system. At the beginning, the probe is far from the substrate hence we do not see any interaction. We then bring the probe in contact with the substrate. While in contact one can change the duration that the probe and substrate are in contact, which we call the contact time t_c. The force-distance $F - d$ curves can also be affected by the speed by which the probe retracts, retraction speed v_r. These last two variables are our main experimental probes. Upon approaching and retracting of the probe to the substrate, we determine the spatial variation of the probe–substrate interaction by recording the F-d curves at a large number of sample surface locations. We observed a typical F–d curve obtained from one of our measurements in Fig. 8 that schematically shows different regions of a F–d curve. Approach and retract curves can be divided roughly into three regions: the contact line, the non-contact region and the zero line. The zero line is obtained when the probe is far from the substrate and the cantilever deflection is close to zero. When the substrate is pressed against the probe, the corresponding cantilever deflection plot is called the contact line and this line can provide information on sample stiffness. The most interesting regions of the F–d curve are two regions, containing the jump-to-contact and the jump-off-contact. The non-contact region in the approach curve gives information about attractive (van der Waals or Coulombic forces) or

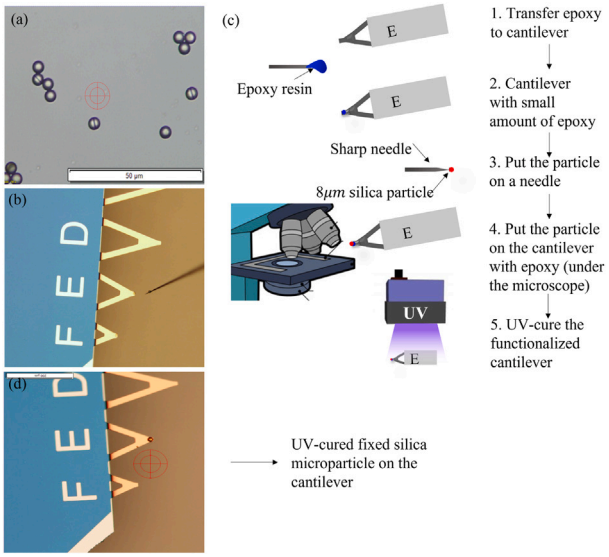

Fig. 7. The steps of gluing a silica microparticle on a cantilever: (a) 8 μm silica particles under the microscope, (b) deposition of the silica microparticle to the top of the cantilever E using a sharp needle made of a tungsten wire, and (c) the steps of transferring UV curable epoxy to cantilever and depositing the silica microparticle, and (d) the UV-cured functionalized cantilever which is ready to be used for the force spectroscopy measurements.

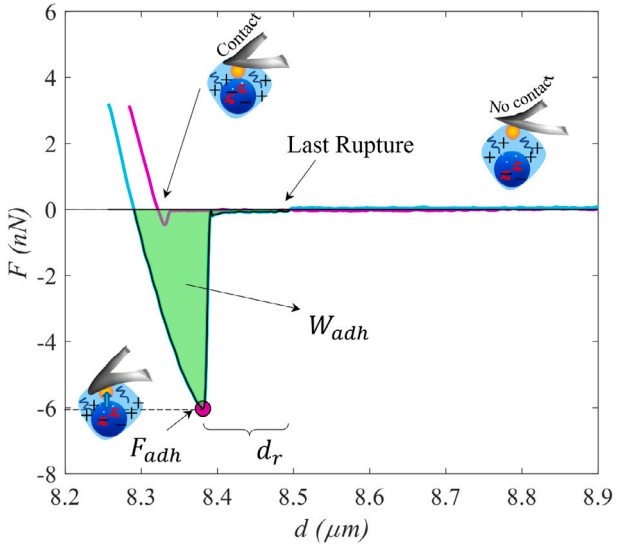

Fig. 8. A typical F-d curve. Three regions of no contact, contact point and pull-off are shown with the schematics from right to left. The approach and retraction curves are both shown. We can extract different properties from this plot, such as the minimum point which is defined as the adhesion force F_{adh}, the area under the curve which is work of adhesion W_{adh}, and rupture distance d_r which is the distance from the last rupture to the peak adhesion point.

repulsive forces (van der Waals in some liquids, double-layer, hydration and steric force) before contact; this discontinuity occurs when the gradient of the probe–substrate force exceeds the spring constant of the cantilever. The non-contact region in the retract curve contains the jump-off-contact, a discontinuity that occurs when the cantilever's spring constant is greater than the gradient of the probe–substrate (adhesion force F_{adh}) (Fig. 8). We determine the work of adhesion W_{adh} by integrating the area under the F–d curve and can be expressed by several continuum contact mechanics theories, or modern molecular dynamics calculations that have been the source of many important insights into nano-scale mechanics. Such theoretical comparisons are beyond the scope of the current work.

Adhesion is governed by short-range intermolecular forces which in many cases can be controlled by appropriate surface modification. This provides a specific chemical functionality on the probe surface. The functionalized tips can then be used in F–d curve measurements. The general idea, in this case, is to probe the adhesion forces between the probe and the substrate. We measure at least 20 force curves on two areas on the sample surfaces. Here as controlling parameters, we change the pH of the solvent (pH=3,7,11), contact time (t_c=0–40 s), and retraction speed (v_r=0.2-5 μm s^{-1}). In the next sections we will describe to what extent these parameters affect the interaction between the particles and hence the adhesion force.

3. Results and discussion

3.1. Bulk interaction of ceramic suspension

We study adhesive dynamics of the ceramic particles suspension by changing pH of the suspension. The dramatic impact of fluid chemistry on modifying suspension rheology and adhesive interactions has previously been demonstrated in the case of a shear-thickening cornstarch suspension [37]. Le et al. have identified several particle-level mechanisms responsible for alterations in rheology and microscopic friction as the fluid or solvent undergoes changes. One primary mechanism involves the swelling of particles within the solvent, where the solvent penetrates and induces particle size increase. This results in the creation of a swollen polymer layer, forming a polymer brush that extends over the particle's surface. Consequently, this polymer brush leads to the emergence of long-range steric repulsion forces [38]. The presence of a surfactant can also modify the interplay between adhesion and load-dependent friction properties, affecting the shear-thinning behavior of non-Brownian suspensions [39].

Through flow curves we investigate the pH and rate dependency in the bulk. We perform rheology measurements in three intervals: shear stress ramp, amplitude sweep and frequency sweep tests. Using the shear stress ramp measurements we can specify the cohesiveness of the suspension at different pH values. Fig. 9 shows the viscosity η as a function of the shear rate $\dot{\gamma}$ obtained from the shear stress ramp measurements for three acidic, neutral and basic environments. At all pH values viscosity η decreases with the shear rate $\dot{\gamma}$. The slope of the flow curve at low $\dot{\gamma}$ is approximately −1, suggesting that the suspension is sedimented and with predominantly long-lasting, frictional contacts. At pH=3 viscosity η is higher by approximately an order of magnitude so that the suspension is more paste-like due to the likely adhesive contacts. The pH=7 and 11 shows almost the same but lower viscosity through all rates. At increasing $\dot{\gamma}$, the flow curves for various pH suspensions begin to coincide, suggesting a transition to flow without enduring contacts, but rather a viscous or inertial flow regime [40].

Indeed, the reduction in apparent viscosity can stem from various sources. It may result from resuspension or even intrinsic shear-thinning at a constant ϕ (volume fraction) of the suspension. In order to gain deeper insights into the shear-thinning characteristics of the suspension, we conducted a series of rheology experiments using a plate-plate geometry (Fig. 10). We used a plate with a diameter of 50 mm for our experiments. To prevent evaporation in the suspension, a solvent trap was employed. Additionally, we affixed sandpaper to the plates to establish no-slip boundary conditions. Our experimental procedure involved conducting a steady shear rate ramp, involving both decreasing and increasing shear rates. As depicted in Fig. 10, we observed a consistent decreasing trend in viscosity as the shear rate increased. This behavior aligns with our previous observations using the vane-cup geometry, confirming the shear-thinning behavior exhibited by our suspension.

We study the visco-elasticity of the suspension through oscillation measurements. We describe the deformation behavior of the suspension

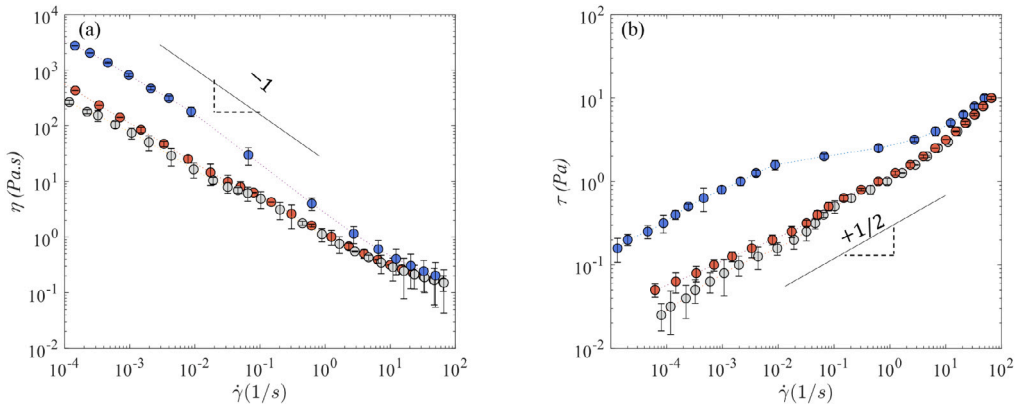

Fig. 9. (a) Viscosity η and (b) shear stress τ as a function of the shear rate $\dot{\gamma}$ at pH=3 ····●····, pH=7 ····○····,pH=11 ····●····. Based on power-law fluid equation $\eta = k\dot{\gamma}^{n-1}$, the slope is $n-1$ and ceramic suspension here is a shear-thinning fluid with $n < 1$.

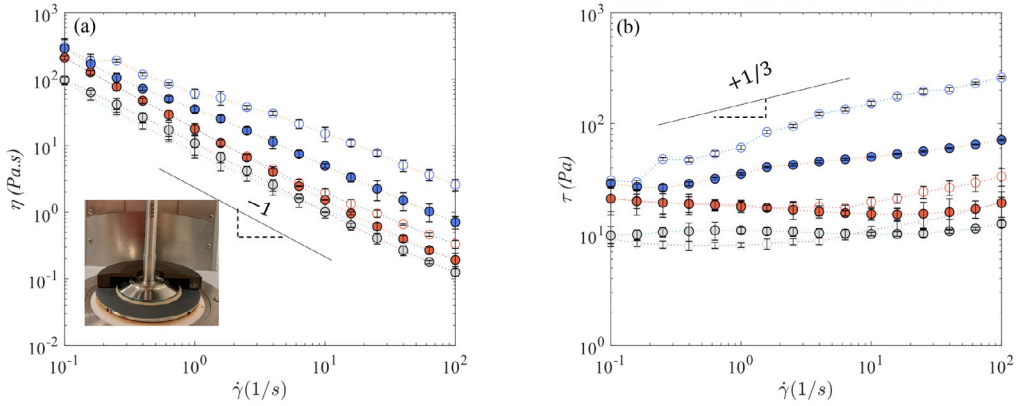

Fig. 10. Steady shear rheology in rough plate-plate geometry, (a)viscosity η and (b) shear stress τ as a function of the shear rate $\dot{\gamma}$ at pH=3 ····●····, pH=7 ····○····,pH=11 ····●····. The solid circles represent forward curves with a decreasing $\dot{\gamma}$ ranging from 100 to 0.1 $1/s$, while the hollow circles represent backward curves with an increasing $\dot{\gamma}$ ranging from 0.1 to 100 $1/s$.

by performing amplitude sweep measurement at constant frequency of $f = 1$ Hz. (G') is shown as a function of the strain γ for different pH (Fig. 11a). We observe higher stored deformation energy G' at pH=3. The length of the linear visco-elastic region (plateau at low strain) indicates the range in which the test can be carried out without destroying the structure of the sample. Here, we do not observe a plateau at the lowest strain ($\gamma = 0.01\%$), so that no real observed linear visco-elastic region. We then choose the lowest strain of $\gamma = 0.01\%$ from Fig. 11a and perform frequency sweep measurement (Fig. 11b). The frequency sweep shows the time-dependent behavior of a sample in the non-destructive deformation range. High frequencies are used to probe fast motion on short timescales, whereas low frequencies probe slow motion on long timescales or at rest. In Fig. 11b, we see a higher G' at pH=3; however, there is not that much of dependency of the (G') on the frequency. We therefore observe that decrease in the pH, leads to an increase in the adhesive properties of the ceramic suspension which is shown in terms of higher viscosity η and higher G'.

3.2. Molecular scale effects: ceramic-silica interaction in aqueous solution

We obtained the $F-d$ plots from the CP-AFM at different contact times t_c (Fig. 12) and retraction speeds v_r (Fig. 13) at pH=3. We mainly show here pH=3 plots as we only see adhesion at pH=3. In both Figs. 12 and 13, there is an increasing trend in the force as a function of t_c and v_r. We determine the peak forces (F_{adh}) from Figs. 12 and 13 and plot it as a function of contact time t_c (Fig. 14a) and retraction speed v_r (Fig. 14c). The isoelectric point for ceramic suspension is approximately in the range of pH=2-4; we assume in the same limit as for the silica particle (ceramic particles contain 70% silica). Therefore, we consider suspension at pH=3 to be below isoelectric point and positively charged. The AFM measurements supports such perspective as they reveal that approaching a single silica bead to a ceramic suspension at pH=3 results in an attractive interaction, probably due to the (likely) electrostatic attraction.

The adhesion force plots reveal different behaviors with the increase of the time of contact t_c (Fig. 14a) and retraction speed v_r Fig. 14c in solution at pH=3. We observe this by increasing t_c from 0 s to 40 s. This presumably means when the particles stay in contact for a longer time, certain (unknown) chemical reactions between the charges of silica and ceramic particles becomes more pronounced and causes the adhesion to increase. For the neutral environment, there is almost no interaction, hence no significant adhesion between the particles. Changing the charge densities by lowering the pH, causes the adhesion to appear between particles. We believe that this is mainly due to reactive silanol groups (Si–OH) and H^+ in water. The formation of adhesive contacts in a specific fluid environment, e.g. where polymer solubility is at its peak, has also been demonstrated to be linked to the macroscopic yield stress [37]. In addition, when two particles are in contact, there is an interface between them with a certain interfacial energy. When the two particles are separated, this interface will disappear but two new are

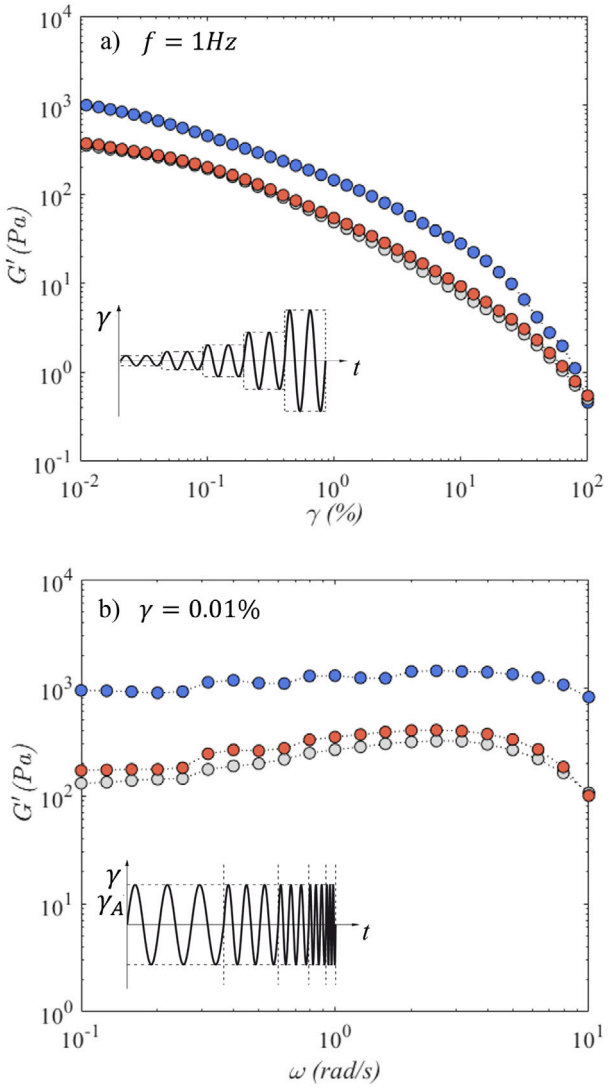

Fig. 11. (a) Amplitude sweep (storage modulus G' as a function of strain γ) at constant frequency of $f = 1$ Hz, and (b) frequency sweep (storage modulus G' as a function of angular frequency ω) at constant strain of $\gamma = 0.01\%$ at pH=3 ····●····, pH=7 ····○····, pH=11 ····●····.

formed. A rise in the interfacial attraction results in an increase in the work of adhesion W_{adh}. Fig. 14b shows an increasing trend of the work of adhesion W_{adh} with contact time t_c. Note that the F–d curves are highly reproducible for a single contact at a given location on a ceramic particle, which rules out significant contact plasticity.

We can estimate the hydrodynamic lubrication forces in both smooth and rough particle–particle interactions. These forces occur when a lubricating fluid separates two surfaces as they move relative to each other. We can use the Reynolds equation to predict the thin film lubrication force ($\approx 6\pi\eta V R/h$). Given the viscosity of water at 25° $\eta = 8.9 \cdot 10^{-4}$ Pa s, the speed of retraction $V = 1$ μm s^{-1}, the radius of the contacting spheres $R = 4$ μm and the scale of roughness based on the surface profilometry data (Fig. 4) with $h \approx 120$ μm, we can estimate the lubrication force $F_{lub} \approx 0.6$ nN, while noting that also the thin film approximation of $h \ll R$ breaks down. We conclude that these forces were relatively insignificant and did not play a major role in the interactions between the particle surfaces.

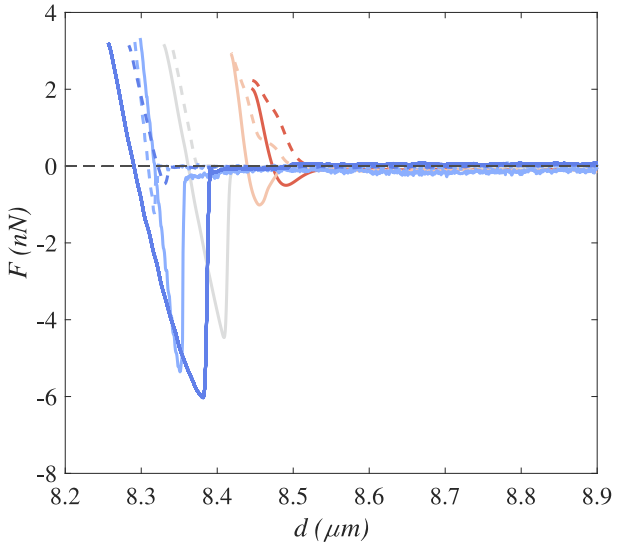

Fig. 12. The F-d curve at different contact times $t_c = 0$ s ——, $t_c = 0.5$ s ——, $t_c = 1$ s ——, $t_c = 4$ s ——, $t_c = 40$ s —— at a constant retraction speed $v_r = 1$ μm s^{-1} at pH=3. Here both approach - - - and retract —— lines are shown.

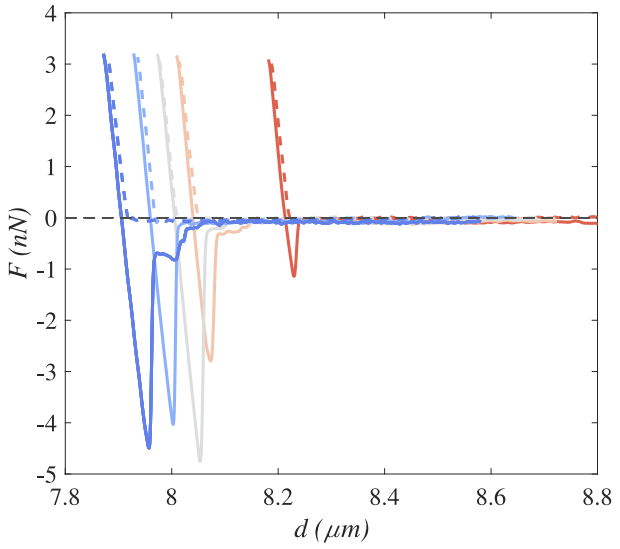

Fig. 13. The F-d curve at different retraction speed $v_r = 0.2$ μm s^{-1} ——, $v_r = 0.6$ μm s^{-1} ——, $v_r = 0.8$ μm s^{-1} ——, $v_r = 1$ μm s^{-1} ——, $v_r = 5$ μm s^{-1} —— at constant contact time $t_c = 1$ s at pH=3. Here both approach - - - and retract —— lines are shown.

Even though hydrodynamic effects may be neglected at these length and time scales, another timescale that can influence the adhesion force and compete with the shear rate in a flowing suspension is the speed by which the contacting particles retract to snaps away from the surface — we call this v_r. We observe that when the cantilever retracts faster, the energy that is required to pull-off the cantilever from the substrate is higher, and therefore the energy dissipation is higher (Fig. 14c). This is all valid for the acidic environment. At acidic environment pH=3,

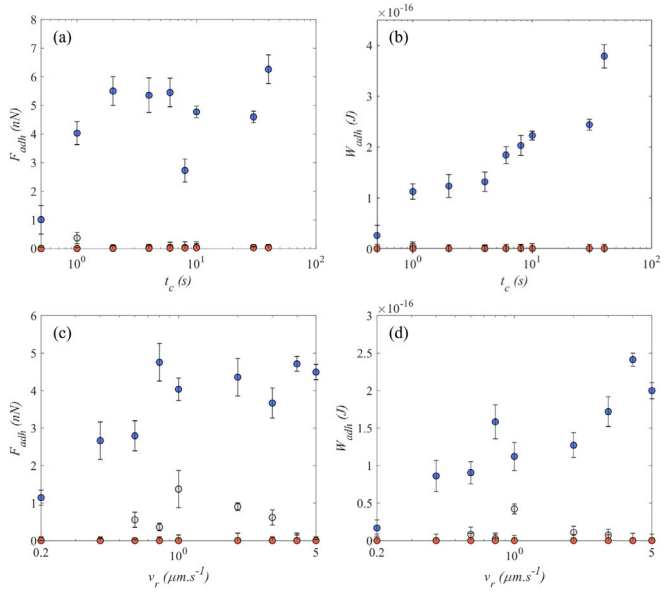

Fig. 14. (a) Adhesion force F_{adh} as a function of contact time t_c, (b) corresponding work of adhesion W_{adh} as a function of contact time t_c. (c) Adhesion force F_{adh} as a function of retraction speed v_r, and (d) corresponding work of adhesion W_{adh} as a function of retraction speed v_r at pH=3 ●, pH=7 ○,pH=11 ●. Error bars show the standard deviation of 20 measurements.

when we increase the v_r to 1 μm s^{-1} there is a jump in F_{adh} to 5 nN and adhesion remains almost constant up to the 5 μm s^{-1}. However, if we look at the work of adhesion W_{adh}, we observe that the work of adhesion is increasing with retraction speed (Fig. 14d). The specific mechanism behind a retraction speed dependence is not obvious in this context.

4. Discussion

We have demonstrated the effect of cohesiveness of the ceramic particle suspension on the micro and macro-scale flow curves. At the macro level, we performed rheology measurements and specified the cohesiveness of the suspension at different pH values. We observed a shear thinning fluid behavior in ceramic suspension. When we lower the pH of the suspension, we observed an increase in the viscosity η. We believe at pH=3 there is an adhesive contacts forming between the particles which forces the suspension to become more sticky by increasing H^+. However pH=7 and 11 shows almost the same but lower viscosity through all rates, and hence only frictional dissipation can be seen there.

The adhesion force plots reveal different behaviors with the increase of the time of contact t_c and retraction speed v_r in an acidic solution. Changing the charge densities by lowering the pH, causes the adhesion to appear between particles. We believe that this is mainly due to the chemical reactions at the surface of silica and ceramic particles between reactive silanol groups (Si–OH) and H^+ in water. When two particles are in contact, there is an interface between them with a certain interfacial energy. JKR theory would suggest that $F_{adh} \propto W_{adh}$. We do not see such a clear trend, but close inspection of pull-off data reveals multiple separate detachment events, which can cause a breakdown of this proportionality: multiple (slowly grown) bonded surfaces appear to rupture during these pull-off process. While these fluctuations can be seen in the adhesion force data, the work of adhesion always shows an increasing trend with t_c and v_r. We conclude that W_{adh} is a better parameter to quantify the adhesion behavior than the peak force.

5. Conclusions

We link molecular-scale to macro-scale adhesive behavior of the ceramic microparticles. We used colloidal-probe atomic force microscopy CP-AFM and rheometric measurements to study the effect of pH, contact time t_c, and rate dependency v_r of the adhesion forces between the particles. We conclude that the adhesion force is strongly dependent on the surface chemistry of the tested particles. Based on the surface chemistry and the chemical reactions that occur between the particles, different adhesive response can be measured through force-distance curves. In all cases we see the dependency of the adhesion force to pH, contact time t_c and retraction speed v_r. We showed that acidic environment plays an important role in increasing the stickiness of the particles and that the adhesion timescales compete with the shear rate to affect rheology. This interesting behavior of the ceramic particles may bring further insights to help to compare how their adhesive particle-level properties affect macroscopic flow behavior, e.g. to use this feature for further applications in the industrial processing such as tile production in ceramic industry.

CRediT authorship contribution statement

Zohreh Farmani: Conceptualization, Data curation, Formal analysis, Investigation, Methodology, Validation, Writing – original draft, Writing – review & editing. **Joshua A. Dijksman:** Formal analysis, Funding acquisition, Project administration, Supervision, Writing – review & editing.

Declaration of competing interest

The authors declare the following financial interests/personal relationships which may be considered as potential competing interests: Joshua A. Dijksman reports some materials were provided by Sacmi Imola SC.

Data availability

Data will be made available on request.

Acknowledgments

This project has received funding from the European Union's Horizon 2020 research and innovation programme under the Marie Skłodowska-Curie grant agreement CALIPER No 812638. Xiufeng Li is acknowledged for important contributions to the training of the AFM setup and helpful discussions. We acknowledge Riccardo Cenni, Ibanez Riccò and Stefano Maretti from SACMI company for supplying particles and fruitful discussions.

References

[1] Jonathan J. Stickel, Robert L. Powell, Fluid mechanics and rheology of dense suspensions, Annu. Rev. Fluid Mech. 37 (2005) 129–149.
[2] Guillaume Chatté, Jean Comtet, Antoine Nigues, Lydéric Bocquet, Alessandro Siria, Guylaine Ducouret, François Lequeux, Nicolas Lenoir, Guillaume Ovarlez, Annie Colin, Shear thinning in non-Brownian suspensions, Soft Matter 14 (6) (2018) 879–893.
[3] Adolfo Vázquez-Quesada, Roger I. Tanner, Marco Ellero, Shear thinning of noncolloidal suspensions, Phys. Rev. Lett. 117 (10) (2016) 108001.
[4] Adolfo Vázquez-Quesada, Arif Mahmud, Shaocong Dai, Marco Ellero, Roger I. Tanner, Investigating the causes of shear-thinning in non-colloidal suspensions: Experiments and simulations, J. Non-Newton. Fluid Mech. 248 (2017) 1–7.
[5] Anastasia Papadopoulou, Jurriaan J. Gillissen, Helen J. Wilson, Manish K. Tiwari, Stavroula Balabani, On the shear thinning of non-Brownian suspensions: Friction or adhesion? J. Non-Newton. Fluid Mech. 281 (2020) 104298.
[6] Laurent Lobry, Elisabeth Lemaire, Frédéric Blanc, Stany Gallier, François Peters, Shear thinning in non-Brownian suspensions explained by variable friction between particles, J. Fluid Mech. 860 (2019) 682–710.
[7] F. Gadala-Maria, Andreas Acrivos, Shear-induced structure in a concentrated suspension of solid spheres, J. Rheol. 24 (6) (1980) 799–814.

[8] Roger I. Tanner, Christopher Ness, Arif Mahmud, Shaocong Dai, Jiyoung Moon, A bootstrap mechanism for non-colloidal suspension viscosity, Rheol. Acta 57 (2018) 635–643.
[9] Asal Amiri, Gisle Øye, Johan Sjöblom, Stability and flow-induced flocculation of fumed silica suspensions in mixture of water-glycerol, J. Dispers. Sci. Technol. 33 (8) (2012) 1247–1256.
[10] Efstathios Kaliviotis, Michael Yianneskis, On the effect of dynamic flow conditions on blood microstructure investigated with optical shearing microscopy and rheometry, Proc. Inst. Mech. Eng., Part H: J. Eng. Med. 221 (8) (2007) 887–897.
[11] Aaron PR Eberle, Nicos Martys, Lionel Porcar, Steven R. Kline, William L. George, Jung M. Kim, Paul D. Butler, Norman J. Wagner, Shear viscosity and structural scalings in model adhesive hard-sphere gels, Phys. Rev. E 89 (5) (2014) 050302.
[12] Francesco Bonacci, Xavier Chateau, Eric M. Furst, Jennifer Fusier, Julie Goyon, Anaël Lemaître, Contact and macroscopic ageing in colloidal suspensions, Nature Mater. 19 (7) (2020) 775–780.
[13] Francesco Bonacci, Xavier Chateau, Eric M. Furst, Julie Goyon, Anaël Lemaître, Yield stress aging in attractive colloidal suspensions, Phys. Rev. Lett. 128 (1) (2022) 018003.
[14] Raffaella Martone, Claudia Carotenuto, Mario Minale, Non-Brownian Newtonian suspensions may be rate dependent in time sweep oscillatory shear flow, J. Rheol. 64 (5) (2020) 1075–1085.
[15] Joannes Mewis, Flow behaviour of concentrated suspensions: predictions and measurements, Int. J. Miner. Process. 44 (1996) 17–27.
[16] Haisheng Chen, Wei Yang, Yurong He, Yulong Ding, Lingling Zhang, Chunqing Tan, Alexei A. Lapkin, Dmitry V. Bavykin, Heat transfer and flow behaviour of aqueous suspensions of titanate nanotubes (nanofluids), Powder Technol. 183 (1) (2008) 63–72.
[17] Zhouzun Xie, Shuai Wang, Yansong Shen, CFD-DEM modelling of the migration of fines in suspension flow through a solid packed bed, Chem. Eng. Sci. 231 (2021) 116261.
[18] Enzu Zheng, Murray Rudman, Shibo Kuang, Andrew Chryss, Turbulent coarse-particle suspension flow: Measurement and modelling, Powder Technol. 373 (2020) 647–659.
[19] Bert Voigtländer, Atomic Force Microscopy, Springer, 2019.
[20] Johann Erath, Stephan Schmidt, Andreas Fery, Characterization of adhesion phenomena and contact of surfaces by soft colloidal probe AFM, Soft Matter 6 (7) (2010) 1432–1437.
[21] Hans-Jürgen Butt, Brunero Cappella, Michael Kappl, Force measurements with the atomic force microscope: Technique, interpretation and applications, Surface Sci. Rep. 59 (1–6) (2005) 1–152.
[22] Franz J. Giessibl, Advances in atomic force microscopy, Rev. Modern Phys. 75 (3) (2003) 949.
[23] F.L. Leite, P.S.P. Herrmann, Application of atomic force spectroscopy (AFS) to studies of adhesion phenomena: A review, J. Adhes. Sci. Technol. 19 (3–5) (2005) 365–405.
[24] F.L. Leite, L.H.C. Mattoso, O.N. Oliveira, P.S. de P. HERRMANN JUNIOR, The atomic force spectroscopy as a tool to investigate surface forces: Basic principles and applications, Embrapa Instrumentação-Capítulo em livro científico (ALICE) (2007).
[25] Aleksandr Noy, Chemical force microscopy of chemical and biological interactions, Surf. Interface Anal.: Int. J. Devoted Dev. Appl. Tech. Anal. Surf., Interfaces Thin Films 38 (11) (2006) 1429–1441.
[26] Quy K. Ong, Igor Sokolov, Attachment of nanoparticles to the AFM tips for direct measurements of interaction between a single nanoparticle and surfaces, J. Colloid Interface Sci. 310 (2) (2007) 385–390.
[27] Justine Laurent, Audrey Steinberger, Ludovic Bellon, Functionalized AFM probes for force spectroscopy: Eigenmode shapes and stiffness calibration through thermal noise measurements, Nanotechnology 24 (22) (2013) 225504.
[28] Rong An, Aatto Laaksonen, Muqiu Wu, Yudan Zhu, Faiz Ullah Shah, Xiaohua Lu, Xiaoyan Ji, Atomic force microscopy probing interactions and microstructures of ionic liquids at solid surfaces, Nanoscale 14 (31) (2022) 11098–11128.
[29] W. Richard Bowen, Nidal Hilal, Robert W. Lovitt, Chris J. Wright, An atomic force microscopy study of the adhesion of a silica sphere to a silica surface—effects of surface cleaning, Colloids Surf. A 157 (1–3) (1999) 117–125.
[30] Adam Feiler, Paul Jenkins, John Ralston, Metal oxide surfaces separated by aqueous solutions of linear polyphosphates: DLVO and non-DLVO interaction forces, Phys. Chem. Chem. Phys. 2 (24) (2000) 5678–5683.
[31] A. Filby, M. Plaschke, H. Geckeis, AFM force spectroscopy study of carboxylated latex colloids interacting with mineral surfaces, Colloids Surf. A 414 (2012) 400–414.
[32] Sameh Obeid, Fanny Guyomarc'h, Grégory Francius, Herve Guillemin, Xiaoxi Wu, Stéphane Pezennec, Marie-Hélène Famelart, Chantal Cauty, Frédéric Gaucheron, Christelle Lopez, The surface properties of milk fat globules govern their interactions with the caseins: Role of homogenization and pH probed by AFM force spectroscopy, Colloids Surfaces B 182 (2019) 110363.
[33] Thomas Mezger, The Rheology Handbook: For Users of Rotational and Oscillatory Rheometers, European Coatings, 2020.
[34] B.J. Dobraszczyk, M.P. Morgenstern, Rheology and the breadmaking process, J. Cereal Sci. 38 (3) (2003) 229–245.
[35] Norman Y. Yao, Ryan J. Larsen, David A. Weitz, Probing nonlinear rheology with inertio-elastic oscillations, J. Rheol. 52 (4) (2008) 1013–1025.
[36] Bent Babel, Martin Rudolph, Characterizing mineral wettabilities on a microscale by colloidal probe atomic force microscopy, Miner. Eng. 121 (2018) 212–219.
[37] Loreto Oyarte Gálvez, Sissi de Beer, Devaraj van der Meer, Adeline Pons, Dramatic effect of fluid chemistry on cornstarch suspensions: Linking particle interactions to macroscopic rheology, Phys. Rev. E 95 (3) (2017) 030602.
[38] Anh Vu Nguyen Le, Adrien Izzet, Guillaume Ovarlez, Annie Colin, Solvents govern rheology and jamming of polymeric bead suspensions, J. Colloid Interface Sci. 629 (2023) 438–450.
[39] Muhammad Arshad, Abdelhamid Maali, Cyrille Claudet, Laurent Lobry, Francois Peters, Elisabeth Lemaire, An experimental study on the role of inter-particle friction in the shear-thinning behavior of non-Brownian suspensions, Soft Matter 17 (25) (2021) 6088–6097.
[40] Élisabeth Guazzelli, Olivier Pouliquen, Rheology of dense granular suspensions, J. Fluid Mech. 852 (2018) P1.